Research Paper
J. Astron. Space Sci. 42(1), 29-37 (2025)
https://doi.org/10.5140/JASS.2025.42.1.29

JASS Journal of Astronomy and Space Sciences

Trends of Solar, Interplanetary, and Geomagnetic Parameters during the Recent Five Solar Cycles

Myunghwan Kim[1,2], Suyeon Oh[3†]

[1]Gwangju Science Academy for the Gifted, Gwangju 61005, Korea
[2]Department of Science Education, Chonnam National University, Gwangju 61186, Korea
[3]Department of Earth Science Education, Chonnam National University, Gwangju 61186, Korea

This study examined the variations of solar, interplanetary, and geomagnetic (SIG) parameters from 1974 to 2024 to assess the changes in the solar cycle. Eleven SIG parameters were analyzed, including the sunspot number (SSN), solar magnetic field, 10.7 cm solar radio flux, total solar irradiance, and Ap index. This study also aimed to predict Solar Cycle 25 using the seasonal autoregressive integrated moving average (SARIMA) statistical forecasting model. The results showed that consistent with previous studies, all SIG parameters exhibited a strong correlation with the SSN. The change in SSN strongly influences the variations in all SIG parameters, even though some exhibit time-lagged responses. The cross-correlation analysis revealed a high correlation coefficient of 0.9678 between the SSN and the 10.7 cm solar radio flux without delay. Most SIG parameters showed a general weakening trend toward Solar Cycles 22–24. This suggests that solar activity is waning over time. In particular, the solar polar magnetic field (SPMF) showed a large decrease in the solar minimum 23/24, and specifically, the SPMF at the south pole weakened more rapidly than at the north pole. Hence, the SPMF is changing asymmetrically between the north and south poles. This weakening of the solar magnetic field suggests an increase in galactic cosmic rays within the heliosphere, exposing the Earth to higher levels of cosmic rays. Finally, forecasts for Solar Cycle 25 using the SARIMA model predict that the SSN will continue to decline after the solar maximum in 2024, with the predicted minimum SSN of 9.42 in October 2028, and will likely enter a solar minimum period around 2030.

Keywords: sunspot number, solar cycle, SIG parameters, prediction, SARIMA model

1. INTRODUCTION

Solar magnetic fields are formed from a combination of the internal convection of plasma and differential rotation. The plasma-filled Sun has different rotational speeds depending on the latitude. This differential rotation pulls and pushes the internal plasma, forming a magnetic field. This magnetic field becomes twisted and complicated, which drives the various magnetic phenomena on the solar surface and atmosphere.

The solar activity indicates variations or phenomena related to the solar magnetic field. The strength of the magnetic field varies periodically or transiently. This variation in the solar magnetic field leads to various solar activities, including sunspots, solar flares, prominences, coronal mass ejections, solar winds, and the eruption of solar energetic particles.

The sunspot number (SSN), an index representing solar activity, increases and decreases every 11 years, called the solar cycle (sunspot cycle and solar activity cycle). The 11-yr cycle of the SSN was first recognized by Schwabe (1843). Rudolf Wolf analyzed the past sunspot data to study the solar cyclic variations and prepared a formula to count the SSN systematically. Following Wolf's tradition, 1755–1766 was defined as the first solar cycle. During the 11-yr cycle, the solar maximum and minimum are when the SSN is at its

Received 20 JAN 2025 **Revised** 17 FEB 2025 **Accepted** 27 FEB 2025
†**Corresponding Author**
Tel: +82-62-530-2517, E-mail: suyeonoh@jnu.ac.kr
ORCID: https://orcid.org/0000-0002-6786-620X

maximum and minimum, respectively. The solar activity is strong and weak at the solar maximum (sunspot maximum) and minimum (sunspot minimum), respectively. Each solar cycle contains the time from the solar minimum to the following minimum.

The amounts of radio, extreme ultraviolet, and X-ray radiation increase significantly at the solar maximum. Solar magnetic activity, represented by sunspots, is an important factor in space weather and determining the corona and solar wind characteristics.

The solar, interplanetary, and geomagnetic (SIG) parameters include the solar activity index, solar wind speed, density, interplanetary magnetic field (IMF), and geomagnetic storms. They are important in explaining the solar-terrestrial interaction (Oh & Kim 2013). They are also helpful for evaluating the status of solar activity and the changes in the space environment. In addition, they are essential for predicting space weather, analyzing the response of the terrestrial magnetosphere, and understanding the complicated solar-terrestrial interaction.

Oh & Kim (2013) analyzed the SIG parameters, including SSN, 10.7 cm solar radio flux, total solar irradiance (TSI), solar polar magnetic field (SPMF), and solar mean magnetic field (SMMF). They showed low values for the SIG parameters during Solar Cycles 23–24 and suggested that a reduced solar magnetic field caused these weakened SIG parameters. In addition, they reported that this period showed decreased solar activity compared to the previous solar cycles. They warned that this trend may indicate the onset of a grand minimum, such as the Maunder Minimum, which manifested as markedly low solar activity.

Adhikari et al. (2019) explained that solar activity shows different variations in each solar cycle, and the solar activity in Solar Cycle 24 was remarkably lower than in previous solar cycles. They suggested that the magnetic structure that erupted from a large sunspot group drove the geomagnetic storm, and the magnitude of solar activity determined the effectiveness of space weather near the Earth. In addition, they suggested that future solar activity maintain a lower level than the present.

Nandy (2021) reported the results of the prediction on Solar Cycle 25, which were performed by various research groups using various prediction methods, including the surface flux transport and machine learning model. The maximum SSN was predicted to be in the range of approximately 135–146, and the maximum solar activity was forecasted for the period of 2024–2025.

Xu et al. (2024) made a promising achievement in predicting the solar cycle using the hybrid model to combine the seasonal autoregressive integrated moving average (SARIMA) model and random forest. This hybrid model can provide a more precise prediction than the previous statistical model. It predicted that solar activity in Solar Cycle 25 would be stronger than in Solar Cycle 24 and reach the solar maximum in 2025. In September. 15, 2020, the National Aeronautics and Space Administration (NASA) declared the start of Solar Cycle 25 to be December 2019 (https://www.nasa.gov/news-release/solar-cycle-25-is-here-nasa-noaa-scientists-explain-what-that-means/).

The solar cycle significantly affects space weather on the Earth. Accordingly, monitoring satellites, air traffic, and electrical grids has become important. The solar magnetic field plays an important role in analyzing the effects on the Earth and other planets and contributes to solving various problems related to the space environment. In particular, monitoring and predicting the solar magnetic activity continuously is essential to protect satellites, communication systems, and electrical grids. Since solar magnetic activity directly affects daily life, understanding and managing these phenomena have become essential in the space age. As further research on solar magnetic fields progresses, it is expected that the accuracy of solar activity predictions and the safety from catastrophic changes in the space environment will be enhanced.

Therefore, this study analyzed the solar cyclic variation of SIG parameters over 51 years from 1974 to 2024 and evaluated the prediction on Solar Cycle 25 using the statistical forecasting model. This study also included three main research topics.

1. To evaluate the trends and relationship between the SIG parameters by analyzing the variations in the SIG parameters over 51 years. To understand the trend of variation for SIG parameters according to solar cycles.
2. To compare the solar cyclic variations of the SIG parameters at the solar maxima and minima.
3. To predict the variation of solar activity in Solar Cycle 25 based on the variation of SIG parameters in Solar Cycles 21–24.

2. DATA AND METHOD

This study analyzed the various SIG parameters from 1974 to 2024 and the interrelationships between each SIG parameter. Table 1 describes the data used. The table consists of the data used, the start year of the measurements (indicated below the data), and the provider. Most of the SIG parameters include data up to December 2024. This study used the ten SIG parameters analyzed by Oh & Kim (2013), as shown in Table 1. The solar flare index (SFI) was also

Table 1. Description of the data used

Data (start year)	Reference
SSN (1974)	Monthly and yearly: Solar Influences Data Analysis Center (https://www.sidc.be/SILSO/datafiles)
SPMF (1976)	Stanford Solar Observatory (http://wso.stanford.edu)
SMMF (1975)	
X-ray flare (1975)	M-class: NOAA National Centers for Environmental Information (NCEI) (https://www.ngdc.noaa.gov/stp/solar/solarflares.html) ftp://ftp.swpc.noaa.gov/pub/warehouse/
SFI (1976)	Monthly & Yearly: NOAA NCEI (https://www.ngdc.noaa.gov/stp/solar/solarflares.html)
TSI (1976)	Daily composite TSI: Physikalishch-Meteorologisches Observatorium Davos World Radiation Center (ftp://ftp.pmodwrc.ch/pub/data/irradiance/virgo/TSI/TSI_composite/)
F10.7 (1974)	Daily OMNIWEB data: Goddard Space Flight Center (https://omniweb.gsfc.nasa.gov/form/dx1.html)
IMF (1974)	
Dynamic pressure (1974)	
Ap index (1974)	
GCR intensity (1974)	Daily: McMurdo, Jang Bogo, and Oulu neutron monitors (http://neutronm.bartol.udel.edu/, https://www.nmdb.eu/nest/, https://cosmicrays.oulu.fi/)

SSN, sunspot number; SPMF, solar polar magnetic field; SMMF, solar mean magnetic field; SFI, solar flare index; TSI, total solar irradiance; IMF, interplanetary magnetic field; GCR, galactic cosmic ray; NOAA, National Oceanic and Atmospheric Administration.

included in this study. The SFI is an indicator of solar flare activity and is used to evaluate the incidence and intensity of flares, which are powerful radiative explosions of the Sun. Kleczek (1952) first introduced an amount calculated by "the intensity measure of a flare × the duration of a flare in minutes" to quantify the average daily flare activity over one day. He hypothesized that this relationship provides the approximate total energy that a flare emits. Although it is impossible to measure the total energy of a flare, the flare index can be defined using the white light flare associated with Hα.

The National Geophysical Data Center (NGDC) defined the SFI as "the importance factor of a flare (i) × the duration of a flare (in minutes)". The importance factor of a flare consists of the area of the flare (S, 1, 2, 3, and 4) and the brightness of the flare (**F**aint, **N**ormal, and **B**right; Özgüç et al. 2003). This number can be understood as a relative value indicating how frequent and powerful the flare activity was. The SFI data are provided by the data center operated by the National Oceanic and Atmospheric Administration (NOAA).

The galactic cosmic ray (GCR) intensity refers to the flux of high-energy charged particles flowing from outside the Galaxy. GCR particles are composed mainly of particles arising from high-energy celestial events within the galaxy, such as supernova explosions, which flow into the Earth and the solar system across outer space. GCR particles usually comprise protons (~85%) and helium nuclei (~14%), including heavy element nuclei and electrons. The intensity of GCR particles can be measured by observing secondary particles (e.g., neutrons and muons) generated by their interaction with the Earth's atmosphere, which were detected on the ground. In particular, the changes in GCR intensity reflecting the solar activity can be analyzed using a ground-based neutron monitor. The GCR data of global neutron monitors can be obtained from the data network in NMDB (https://www.nmdb.eu/nest/). This study used the daily averaged data provided by the McMurdo and Jang Bogo neutron monitors. The Jang Bogo neutron monitor took over the observations of the McMurdo neutron monitor in December 2015 (Jung et al. 2016; Jeong & Oh 2022). In addition, GCR data of the Oulu neutron monitor were analyzed as comparative data.

The low-resolution OMNI data set is primarily a 1963-to-current compilation of hourly-averaged, near-Earth solar wind magnetic field and plasma parameter data from several spacecraft in geocentric or L1 orbits. The data have been cross-compared extensively and cross-normalized for some spacecraft and parameters. The daily data of the IMF strength, dynamic pressure, and Ap index are obtained by OMNIWEB (https://omniweb.gsfc.nasa.gov/html/ow_data.html).

The dataset includes SSN (1974), SPMF (1976), absolute SMMF (1975), frequency of X-ray flare (1975), SFI (1975), TSI (1976), 10.7 cm radio flux (F10.7, 1974), IMF (1974), solar wind dynamic pressure (P_{dyn}, 1974), Ap index (1974), and GCR intensity (1974), as shown in Table 1. The solar cyclic variations and the correlations among these parameters were evaluated by processing the data into monthly, yearly, and three-year moving averages (3-yr ave.). The analysis focused on quantifying the variation rate in SIG parameters at solar maxima and minima, providing a quantitative assessment of the solar cycle trends across different cycles.

The solar activity of Solar Cycle 25 was predicted using the SARIMA model provided by Python as a statistical forecasting model. SARIMA combines an autoregressive integrated moving average (ARIMA) model and seasonal components. ARIMA is useful for predicting time series data. SARIMA is a suitable model for predicting periodic data. The SARIMA model analyzes time series data to identify the trends and seasonality. The autoregression (AR), moving average (MA), non-seasonal part of the data (p, d, and q), and seasonal part (P, D, Q, and m) order were set using autocorrelation function (ACF) and partial autocorrelation (PACF) analysis. The formula of the SARIMA model is as follows (Box et al., 2015).

$$SARIMA(p,d,q)(P,D,Q,m),$$

where p, d, and q represent the self-regression order, difference order, and MA order, respectively. P, D, and Q are the seasonal self-regression order, seasonal difference order, and seasonal MA order, respectively. m represents the seasonal cycle. The prediction was performed using the SARIMA model, and the performance was evaluated by comparing it with actual data.

3. RESULTS

3.1 Variation of the Solar, Interplanetary, and Geomagnetic (SIG) Parameters During 51 Years

Fig. 1 presents the solar cyclic variation of ten SIG parameters from 1974 to 2024 arranged in the order of (a) SSN, (b) SPMF magnitude, (c) frequency of M-class solar flare, (d) TSI, (e) 10.7 cm radio flux, (f) absolute SMMF, (g) IMF magnitude, (h) dynamic pressure of solar wind, (i) GCR intensity at McMurdo and Jang Bogo neutron monitors, and (j) Ap index. The monthly mean is plotted with a black solid line, and the yearly mean is drawn with a blue bold line. The red bold line indicates the 3-yr running average of the yearly mean. In Fig. 1(b), the red and blue lines indicate the north and south poles, respectively. All SIG parameters showed a good correlation with solar cyclic variation with the SSN, as reported by Oh & Kim (2013). All SIG parameters remained significantly low from Solar Cycles 22–24 and then recovered slightly at an increasing phase of Solar Cycle 25. The SPMF in Fig. 1(b) shows the lowest value at the transition period from Solar Cycles 23 to 24 and then recovered slightly at the solar minimum from Solar Cycles 24 to 25. On the other hand, the GCR intensity has higher values in the solar minima 23/24 and 24/25 than in the past minima, as shown in Fig. 1(i).

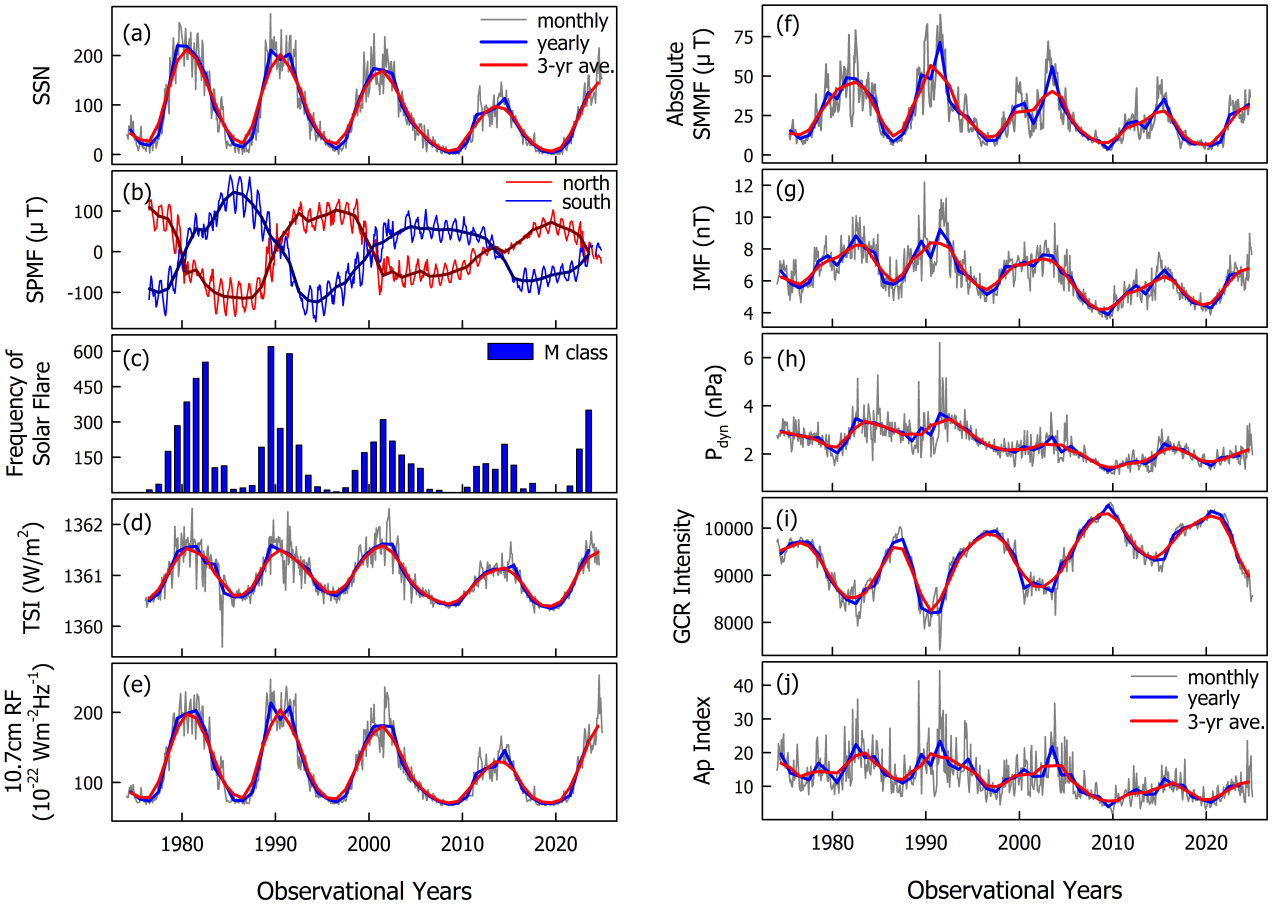

Fig. 1. Solar cyclic variation of ten solar, interplanetary, and geomagnetic (SIG) parameters. (a) sunspot number (SSN), (b) solar polar magnetic field (SPMF) magnitude, (c) frequency of M-class solar flare, (d) total solar irradiance (TSI), (e) 10.7 cm radio flux, (f) absolute solar mean magnetic field (SMMF), (g) interplanetary magnetic field (IMF) magnitude, (h) dynamic pressure of solar wind, (i) galactic cosmic ray (GCR) intensity, and (j) Ap index. The monthly mean is plotted as a black solid line, and the yearly mean is drawn as a blue bold line. The red bold line indicates the three-year running average of the yearly mean. In a plot of the SPMF magnitude (b), red and blue lines indicate the north and south poles, respectively.

Fig. 2 presents the solar cyclic variation of SFI. The display in Fig. 2 is the same as in Fig. 1. The data also showed a good correlation of the solar cyclic variations with the SSN, the same as the other SIG parameters in Fig. 1. The SFI showed a remarkably low level from Solar Cycles 22–24, and then recovers slightly at Solar Cycle 25.

Adhikari et al. (2019) reported that the SSN, 10.7 cm radio flux, and Lyman α emission showed a lower peak at Solar Cycle 24 than in the previous solar cycles. This observation coincides with the results of the present study.

3.2 Variation Rate of Solar, Interplanetary, and Geomagnetic (SIG) Parameters at Solar Maxima and Minima

The variation rate of the SIG parameters at the solar maxima and minima plays an important role in understanding the periodic changes in solar activity. This explains how the SIG parameters change when the solar activity reaches the maximum and minimum. Table 2 lists the start time, end time, and duration of Solar Cycles 21–25 using the three-month running averages.

Table 3 lists the variation rate (%) of ten SIG parameters for Solar Cycles 22–25 at the solar maxima using the yearly averages of the SIG parameters. It compares the SIG parameters between the 22 and 24 solar cycles at the times of solar maxima and * indicates the comparison among solar minima. The solar activity tended to decrease from Solar Cycles 22–24 (Fig. 1), and some SIG parameters showed a significant reduction. A comparison of the solar maxima showed that most of the SIG parameters have the largest decrease in variation rate at Solar Cycle 24 compared to Solar Cycle 22. The GCR intensity showed the largest increase in the variation rate of the McMurdo (Jang Bogo) and Oulu neutron monitors at Solar Cycle 24 compared to Solar Cycle 22. Instead, some SIG parameters (absolute SMMF, SFI, P_{dyn}, and Ap index) show the largest decrease in the variation rate at Solar Cycle 25 compared to Solar Cycle 22. For the solar minima, the greatest variation rate changes showed a decrease in SPMF and an increase in GCR intensity during Solar Cycle 24 relative to Solar Cycle 22.

In particular, the southern SPMF showed a larger decrease than the northern SPMF. Hence, the solar magnetic activity weakens more rapidly in the Southern Hemisphere, leading to asymmetric changes between the magnetic fields of the Northern and Southern Hemispheres.

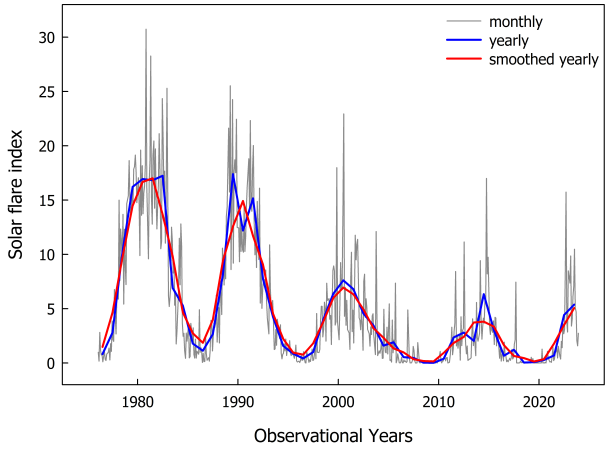

Fig. 2. Solar cyclic variation of the solar flare index (SFI) from 1976 to 2024. The black solid line represents the monthly mean. The blue and red bold lines showed the yearly mean and the smoothed three-year running average, respectively.

Table 2. Start time, end time, and duration of solar cycles 21–25

Solar cycle	Start (minimum)	Maximum	Duration (yr)
21	1976 January	1979 October	11.0
22	1987 January	1989 July	9.2
23	1996 April	2000 July	12.9
24	2009 March	2014 January	10.5
25	2019 October	2024 July*	

* Indicates the preliminary definition of solar maximum.

3.3 Cross-Correlation Analysis of the Solar, Interplanetary, and Geomagnetic (SIG) Parameters

Cross-correlation analysis is a method for analyzing the correlation between two or more time series data. Yan et al. (2012) confirmed a strong correlation between the SSN and SFI by studying their periodic interaction through cross-correlation analysis involving SSN, SFI, and solar radio flux. In addition, Mishra & Mishra (2018) reported that the effect of solar activity on GCR intensity appears with a time lag of several months. Cross-correlation analysis evaluated how early or late one-time series data responds to another. Cross-correlation analysis aims to understand the relationship between two data and the change in correlation over time delay.

Fig. 3 presents the cross-correlation between SSN and 10.7 cm radio flux with respect to the time lag. The X-axis represents the time lag in months, while the Y-axis indicates the correlation coefficient. When the time lag was zero, the correlation coefficient reached its highest value of 0.9783, showing a strong simultaneous relationship between the two parameters. A positive time lag means that the SSN changes first, followed by variations in the 10.7 cm radio flux. Conversely, a negative time lag suggests that the 10.7 cm radio flux changes first, with the SSN responding later. The correlation coefficient falls below 0.75 as the time lag moves away from zero in both positive and negative directions, showing a continuous decrease. This suggests

Table 3. Variation rate (%) of the solar, interplanetary, and geomagnetic (SIG) parameters

SIG parameter	22/23	22/24	22/25	23/24	23/25	24/25
SSN	−17.6	−46.3	−26.8	−34.8	−11.1	36.5
SPMF (N)*	−10.0	−47.2	−36.5	−41.3	−29.5	20.2
SPMF (S)*	−15.3	−61.1	−51.3	−54.1	−42.5	25.3
SMMF	−21.5	−50.2	−55.1	−36.6	−42.8	−9.8
SFI	−56.2	−63.5	−69.1	−16.7	−29.3	−15.1
F10.7	−15.1	−31.6	−10.5	−19.4	5.5	30.9
IMF	−17.3	−27.6	−25.3	−12.6	−9.7	3.3
Pdyn	−26.2	−34.0	−37.7	−10.5	−15.5	−5.6
TSI	2.2×10^{-3}	-2.9×10^{-2}	-7.1×10^{-3}	-3.1×10^{-2}	-9.4×10^{-3}	2.2×10^{-2}
GCR (MCMU)	5.5	13.6	7.7	7.6	2.0	−5.2
GCR (OULU)	6.3	13.5	2.0	6.7	−4.1	−10.2
GCR (MCMU)*	1.7	7.4	6.1	5.5	4.3	−1.2
GCR (OULU)*	1.8	5.8	5.2	4.0	3.4	−0.6
Ap index	−7.2	−47.8	−49.3	−43.7	−45.4	−3.0

Table compares the SIG parameters between the 22 and 24 solar cycles at the times of solar maxima and minima.
* Indicates the comparison among solar minima.
SSN, sunspot number; SPMF, solar polar magnetic field; SMMF, solar mean magnetic field; SFI, solar flare index; IMF, interplanetary magnetic field; TSI, total solar irradiance; GCR, galactic cosmic ray; MCMU, McMurdo neutron monitor; OULU, Oulu neutron monitor.

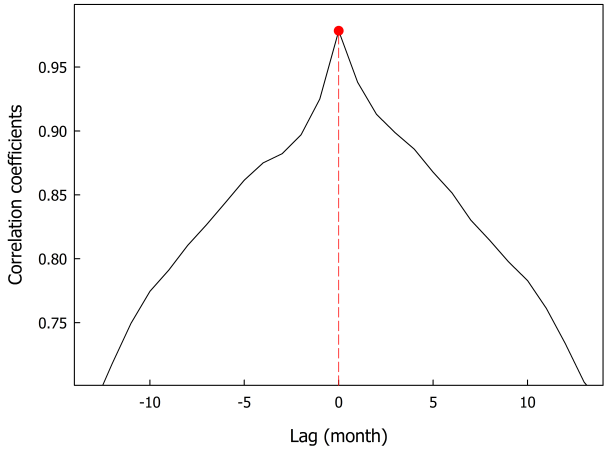

Fig. 3. Cross-correlation coefficients between the sunspot number (SSN) and 10.7 cm radio flux from 1974 to 2024. The red spot and dashed line represent the maximum correlation coefficient and the time lag.

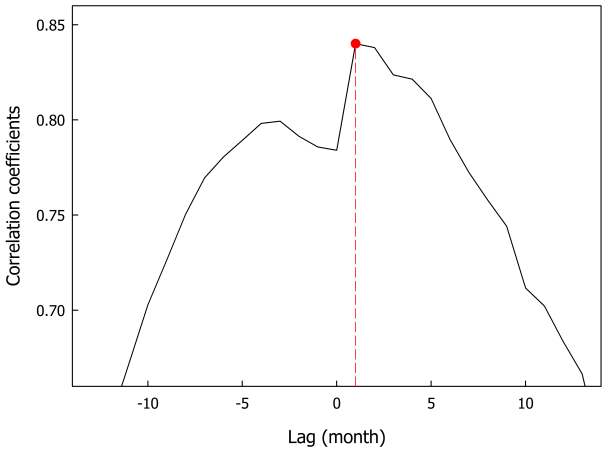

Fig. 4. Cross-correlation coefficients between the sunspot number (SSN) and total solar irradiance (TSI) from 1976 to 2024.

that the relationship between these two parameters weakens progressively as the time lag increases in either direction.

The relationship between the SSN and TSI plays an important role in understanding the interaction between solar activity and radiation emission. Fig. 4 shows the cross-correlation between the SSN and TSI with respect to the time lag, using the same display format as Fig. 3. When the time lag was +1 month, the correlation coefficient reached a peak of approximately 0.8445, suggesting that the TSI responds with a delay of approximately one month following an increase in SSN. Hence, an increase in sunspot activity may lead to a subsequent rise in solar radiation after a short delay. As the time lag increased to +10 months, the correlation coefficient decreased to approximately 0.725, suggesting that the relationship between the two variables weakens over time. The maximum correlation coefficient at a one-month delay is consistent with Privalsky (2021). Privalsky (2021) reported that it is unsuitable for reconstructing the past TSI to apply simple linear regression with the SSN. Hempelmann & Weber (2012) found that the correlation between the SSN and TSI is strongly non-linear. They interpreted this non-linear relationship as the net balance between brightening by faculae dominating at low activity and darkening by sunspots dominating at high activity. Xu et al. (2017) also examined the phase relationships between the SSN and TSI composite data. They reported that the SSN and TSI are positively correlated with time lags of approximately 29 days, which is approximately a solar rotation period. They also confirmed the nonlinearity between SSN and TSI. The non-linear relationship can be explained by the different behaviors and the effects of sunspots, faculae, and the magnetic network.

Therefore, the change in the TSI showed a time lag with the change in the SSN.

Table 4 lists the maximum cross-correlation coefficients between SSN and other SIG parameters and their respective time lags. The highest correlation coefficients with the SSN are shown for the absolute SMMF after six months, SFI with no delay, and IMF after a delay of four months. The solar wind dynamic pressure and Ap index also showed the strongest correlation coefficients after 12 and 11 months, respectively. The GCR intensity showed the highest negative correlation coefficient after eight months.

3.4 Prediction of Solar Cycle 25 Using the Seasonal Autoregressive Integrated Moving Average (SARIMA) Model

NOAA and NASA released the predictions for Solar Cycle 25 from a jointly organized international panel. The panel expects the peak of Solar Cycle 25 to reach July 2025 (± 8 months), and its yearly SSN is predicted to be 115. Compared to Solar Cycle 24, Solar Cycle 25 is expected to proceed with a similar intensity, and the weakening of solar activity is expected to continue in the report of NOAA Space Weather Prediction Center (SWPC; 2020). On the other hand, the monthly SSN for August 2024 was reported to be approximately 216 (the yearly value for 2024 was 155). Hence, the solar activity in Solar Cycle 25 is very active. NOAA/SWPC announced in 2023 that the SSN remained steadily high during 2023, suggesting stronger solar activity than the previous cycle.

A recent study predicted Solar Cycle 25 based on the variation of the solar magnetic field, especially the variations of the SPMF. Solar Cycle 25 was reported to be a relatively strong solar cycle based on the prediction by analyzing the SPMF and geomagnetic index (Penza et al. 2023). In addition, McIntosh et al. (2020) forecasted that Solar Cycle 25 could reach a peak SSN between 210 and 260, suggesting that it may be classified as a particularly strong cycle.

Benson et al. (2020) predicted the SSN by analyzing the SSN data from 1749 to 2019 using a long short-term memory (LSTM) and a WaveNet-based machine learning model. Rodríguez et al. (2022) reported that integrating Fourier transform with machine learning algorithms improves the prediction accuracy compared to conventional forecasting models. These findings highlight the growing importance of Solar Cycle 25 predictions and the application of machine learning techniques in solar cycle analysis.

The SARIMA model explicitly examines the periodicity and periodic variability and allows complex periodic patterns, such as sunspot cycles, to be modeled and predicted. Pandey et al. (2019) used the SARIMA model to predict seasonal and long-term precipitation trends to improve forecast accuracy. Their study revealed the effectiveness of hybrid modeling approaches integrating the SARIMA model for enhanced predictive performance.

The SARIMA model can increase the prediction accuracy by reflecting periodicity. Of course, it is a model suitable for analyzing solar cycles despite the complicated modeling process and the fact that past data may not be sufficiently reflected. In the monthly data, the seasonal cycle (m) of 132 was used to reflect 11 years as the average length of the solar cycle, and the orders were set as follows:

$$(p,d,q)=(1,1,1),(P,D,Q,m)=(1,1,1,132).$$

Fig. 5 shows the predicted SSN for Solar Sycle 25 by the SARIMA model using the monthly SSN for 51 years from 1974 to 2024. The blue and orange lines represent the actual and predicted SSN values, respectively, while the shaded region represents the 95% confidence interval of the forecast. The solar activity over the next 36 months (approximately three years) is expected to decrease gradually. In particular, the SSN is expected to decrease continuously after the solar maximum period, reaching a minimum value of 9.42 in October 2028. It is highly likely to enter the solar minimum period around 2030.

Fig. 6 compares the differences in the SSN prediction between the NOAA SWPC (https://testbed.spaceweather.gov/products/solar-cycle-progression-updated-prediction-experimental) and the SARIMA model during the declining

Table 4. Cross-correlation coefficients between the sunspot number (SSN) and solar, interplanetary, and geomagnetic (SIG) parameters

	SMMF	SFI	10.7 cm radio flux	IMF
Lag (months)	+6	0	0	+4
Cross-correlation	0.7789	0.8501	0.9783	0.7137
	TSI	**Pdyn**	**Ap index**	**GCR intensity**
Lag (months)	+1	+12	+11	+8
Cross-correlation	0.8445	0.3713	0.4822	–0.8282

SMMF, solar mean magnetic field; SFI, solar flare index; IMF, interplanetary magnetic field; TSI, total solar irradiance; GCR, galactic cosmic ray.

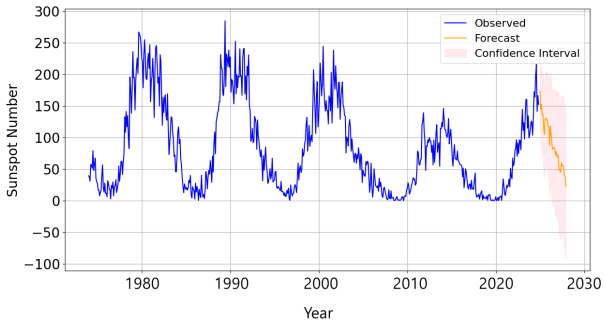

Fig. 5. Predicted sunspot number (SSN) using the seasonal autoregressive integrated moving average (SARIMA) model. The blue and orange lines represent the actual SSN data and the predicted SSN data. The shaded region represents the 95%-confidence interval of the prediction.

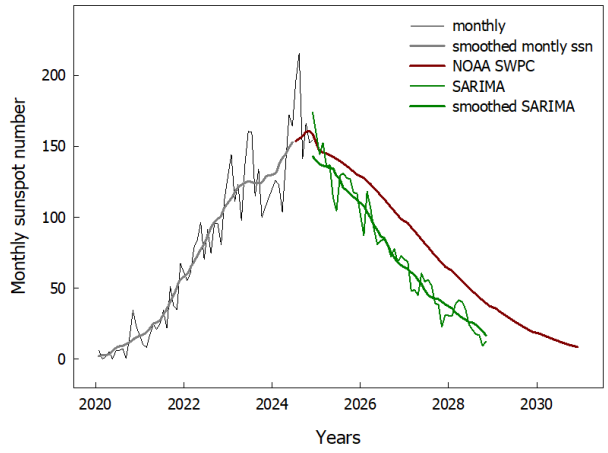

Fig. 6. Comparison of the sunspot number (SSN) prediction in the declining phase for Solar Cycle 25 between the National Oceanic and Atmospheric Administration (NOAA) Space Weather Prediction Center (SWPC) and seasonal autoregressive integrated moving average (SARIMA) model. The black and dark grey bold lines represent the observed monthly and smoothed monthly values, respectively. The dark red bold line indicates the monthly values predicted by the NOAA SWPC, while the green solid and bold lines represent the monthly and smoothed monthly values predicted by the SARIMA model.

phase of Solar Cycle 25. Notably, the predictions of SARIMA model are consistently lower than those of the NOAA SWPC. This discrepancy might be attributed to the reliance of SARIMA model on linear assumptions, which could limit its ability to capture the complex dynamics of solar activity. This suggests that enhancing the model's ability to account for non-linear behaviors may improve the prediction accuracy.

4. SUMMARY AND DISCUSSION

This study analyzed the solar cyclic variation of SIG parameters for 51 years from 1974 to 2024. Based on this, the Solar Cycle 25 was predicted using a statistical forecasting model. The results are summarized as follows.

First, as shown in previous studies, all SIG parameters were closely related to the fluctuations in the solar cycle associated with the SSN. The SIG parameters were correlated according to the solar cycle. Most SIG parameters strongly correlated with the SSN when the solar activity was most active. The SSN is a representative indicator of the solar activity. As the SSN increased, most SIG parameters, such as 10.7 cm radio flux, IMF, SFI, TSI, and solar wind dynamic pressure, increased, but the GCR intensity was inversely proportional to the solar activity.

Second, most SIG parameters showed a general weakening trend toward Solar Cycles 22–24. This suggests that the solar activity waned over time. The SPMF showed a large change in the north and south poles in the Solar Cycle 24. In particular, the southern SPMF weakened more rapidly than the northern SPMF. The SPMF in the northern and southern hemispheres are changing asymmetrically. The GCR intensity tended to increase gradually from Solar Cycles 22 to 24, meaning that the Earth is exposed to more cosmic rays because of the weakening of the solar magnetic field. The parameters of the IMF, TSI, absolute SMMF, 10.7 cm radio flux, SFI, solar wind dynamic pressure, and Ap index tended to be weakened with SSN over time. The difference in the Ap index between Solar Cycles 22 and 24 was quite large, which was attributed to the effect of weakening solar activity on the Earth's magnetic field.

Third, cross-correlation analysis of the SIG parameters showed that the SSN and 10.7 cm radio flux had a maximum correlation coefficient of 0.9678 without delay and a strong correlation. The relationship between the SSN and TSI has a maximum correlation coefficient of approximately 0.8445 after a one-month delay. Hence, the TSI tended to react with an approximately one-month delay after SSN increases. The absolute SMMF, IMF, and GCR intensity show the maximum correlation coefficient after a 4–8 months delay. Most SIG parameters exhibited strong correlations with the SSN, but some displayed delayed responses, such as the TSI and GCR intensity.

Fourth, as a result of predicting the SSN for three years after 2024 by the SARIMA model, the solar activity in the future Solar Cycle 25 is expected to decrease. The minimum SSN was predicted to be 9.42 in October 2028, and it will likely enter a solar minimum period around 2030.

This study attempted to provide important information for understanding the impact of solar activity on the Earth's magnetic field and space environment. The changes in solar activity and space weather can significantly affect the infrastructure on the Earth, particularly satellite communication, electrical grids, aviation, and GPS systems.

The SARIMA model successfully captured the periodic trends in solar activity, but relying on linear assumptions limits its ability to model more complex solar dynamics. Future research should explore advanced machine learning models, such as deep learning and hybrid approaches, to improve long-term solar cycle predictions.

ACKNOWLEDGMENTS

This study was supported by the National Research Foundation of Korea (NRF) grant funded by the Korean government (MSIT) (RS-2023-NR076532). The OMNI data were obtained from the GSFC/SPDF OMNIWeb interface at https://omniweb.gsfc.nasa.gov. The authors thank the WDC-SILSO, Royal Observatory of Belgium, Brussels, for providing sunspot data and the NOAA National Centers for Environmental Information (NCEI) for providing solar flare data. The Wilcox Solar Observatory (WSO) is acknowledged for providing the data on the solar polar magnetic field and solar mean magnetic field. The authors also thank the director of the Oulu neutron monitor (University of Oulu/Sodankyla Geophysical Observatory, https://cosmicrays.oulu.fi/).

ORCIDS

Myunghwan Kim https://orcid.org/0009-0006-2607-5694
Suyeon Oh https://orcid.org/0000-0002-6786-620X

REFERENCES

Adhikari B, Subodh D, Mishra RK, Sapkota N, Chhatkuli DN, et al., Analysis of solar, interplanetary, and geomagnetic parameters during solar cycles 22, 23, and 24. Russ. J. Earth Sci. 19, ES1003 (2019). https://doi.org/10.2205/2018ES000645

Benson B, Pan WD, Prasad A, Gary GA, Hu Q, Forecasting solar cycle 25 using deep neural networks, Sol. Phys. 295, 65 (2020). https://doi.org/10.1007/s11207-020-01634-y

Box GEP, Jenkins GM, Reinsel GC, Ljung GM, Time Series Analysis: Forecasting and Control, 5th ed. (John Wiley & Sons, New York, NY, 2015).

Hempelmann A, Weber W, Correlation between the sunspot number, the total solar irradiance, and the terrestrial insolation, Sol. Phys. 277, 417-430 (2012). https://doi.org/10.1007/s11207-011-9905-4

Jeong J, Oh S, Seasonal trends of the cosmic ray intensity observed by 16 neutron monitors for 1964-2020, Adv. Space Res. 70, 2625-2635 (2022). https://doi.org/10.1016/j.asr.2022.02.052

Jung J, Oh S, Yi Y, Evenson P, Pyle R, et al., Installation of neutron monitor at the Jang Bogo Station in Antarctica, J. Astron. Space Sci. 33, 345-348 (2016). https://doi.org/10.5140/JASS.2016.33.4.345

Kleczek J, Ionospheric disturbances and flares in the 11-year cycle. Bull. Astr. Inst. Czechosl. 3, 52 (1952).

McIntosh SW, Chapman S, Leamon RJ, Egeland R, Watkins NW, Overlapping magnetic activity cycles and the sunspot number: forecasting sunspot cycle 25 amplitude, Sol. Phys. 295, 163 (2020). https://doi.org/10.1007/s11207-020-01723-y

Mishra VK, Mishra AP, Long-term modulation of cosmic-ray intensity and correlation analysis using solar and heliospheric parameters. Sol. Phys. 293, 141 (2018). https://doi.org/10.1007/s11207-018-1357-7

Nandy D, Progress in solar cycle predictions: sunspot cycles 24–25 in perspective, Sol. Phys., 296, 54 (2021). https://doi.org/10.1007/s11207-021-01797-2

Oh S, Kim B, Variation of Solar, interplanetary and geomagnetic parameters during solar cycles 21-24, J. Astron. Space Sci. 30, 101-106 (2013). https://doi.org/10.5140/JASS.2013.30.2.101

Özgüç A, Ataç T, Rybák J, Temporal variability of the flare index (1966–2001), Sol. Phys. 214, 375-396 (2003). https://doi.org/10.1023/A:1024225802080

Pandey PK, Tripura H, Pandey V, Improving prediction accuracy of rainfall time series by hybrid SARIMA–GARCH modeling, Nat. Resour. Res. 28, 1125-1138 (2019). https://doi.org/10.1007/s11053-018-9442-z

Penza V, Bertello L, Cantoresi M, Criscuoli S, Berrilli F, Prediction of solar cycle 25: applications and comparison, Rend. Fis. Acc. Lincei. 34, 663-670 (2023). https://doi.org/10.1007/s12210-023-01184-y

Privalsky V, Application to sunspot numbers and total solar irradiance. in Time Series Analysis in Climatology and Related Sciences (Springer, Wien, 2021), 205-220.

Rodríguez JV, Rodríguez-Rodríguez I, Woo WL, Machine learning-based prediction of sunspots using Fourier transform analysis of the time series, PASP, 134, 124201 (2022). https://doi.org/10.1088/1538-3873/aca4a3

Schwabe HH, Die sonne, Astron. Nachr. 20, 283-286 (1843).

Xu JC, Xie JL, Qu ZN, Phase relations between the sunspot numbers and total solar irradiance, Astrophys. J. 851, 141 (2017). https://doi.org/10.3847/1538-4357/aa9bda

Xu Q, Jain R, Xing W, Data-driven forecasting of sunspot cycles: pros and cons of a hybrid approach. Sol. Phys. 299, 25 (2024). https://doi.org/10.1007/s11207-024-02270-6

Yan XL, Deng LH, Qu ZQ, Xu CL, Kong DF, Phase relationship between sunspot number, flare index and solar radio flux, J. Astrophys. Astron. 33, 387-397 (2012). https://doi.org/10.1007/s12036-012-9153-5